

Long-distance Contributions to Neutrinoless Double Beta Decay

$$\pi^- \rightarrow \pi^+ ee$$

Xin-Yu Tuo,¹ Xu Feng,^{1,2,3,4,*} and Lu-Chang Jin^{5,6,†}

¹*School of Physics, Peking University, Beijing 100871, China*

²*Collaborative Innovation Center of Quantum Matter, Beijing 100871, China*

³*Center for High Energy Physics, Peking University, Beijing 100871, China*

⁴*State Key Laboratory of Nuclear Physics and
Technology, Peking University, Beijing 100871, China*

⁵*Department of Physics, University of Connecticut, Storrs, CT 06269, USA*

⁶*RIKEN-BNL Research Center, Brookhaven National
Laboratory, Building 510, Upton, NY 11973*

(Dated: October 1, 2019)

Abstract

Neutrinoless double beta decay, if detected, would prove that neutrinos are Majorana fermions and provide the direct evidence for lepton number violation. If such decay would exist in nature, then $\pi^-\pi^- \rightarrow ee$ and $\pi^- \rightarrow \pi^+ ee$ (or equivalently $\pi^- e^+ \rightarrow \pi^+ e^-$) are the two simplest processes accessible via first-principle lattice QCD calculations. In this work, we calculate the long-distance contributions to the $\pi^- \rightarrow \pi^+ ee$ transition amplitude using four ensembles at the physical pion mass with various volumes and lattice spacings. We adopt the infinite-volume reconstruction method [1] to control the finite-volume effects arising from the (almost) massless neutrino. Providing the lattice QCD inputs for chiral perturbation theory, we obtain the low energy constant $g_\nu^{\pi\pi}(m_\rho) = -10.89(28)_{\text{stat}}(74)_{\text{sys}}$, which is close to $g_\nu^{\pi\pi}(m_\rho) = -11.96(31)_{\text{stat}}$ determined from the crossed-channel $\pi^-\pi^- \rightarrow ee$ decay [2].

* xu.feng@pku.edu.cn

† ljin.luchang@gmail.com

I. INTRODUCTION

Observation of neutrinoless double beta ($0\nu 2\beta$) decays would prove neutrinos as Majorana fermions and lepton number violation in nature. The light-neutrino exchange is the most widely discussed mechanism to explain $0\nu 2\beta$ decays. Under this mechanism, the decay amplitude is proportional to the effective neutrino mass $m_{\beta\beta}$ and thus the detection of $0\nu 2\beta$ decay would provide the information about the absolute neutrino mass, while the neutrino oscillation experiments are only sensitive to the mass differences among neutrinos.

Due to its importance, the detection of $0\nu 2\beta$ decays is being pursued by many experiments around the world [3–14]. Current experimental measurements of the decay’s half-lives $T_{1/2}^{0\nu}$ have reached the level of $T_{1/2}^{0\nu} > 1.07 \times 10^{26}$ yr for ^{126}Xe [7], with a new generation of ton-scale experiments aiming for the level of sensitivity improved by 1 or 2 orders of magnitude.

On the theoretical side, current knowledge of second-order weak-interaction nuclear matrix elements needs to be improved, as various nuclear models lead to discrepancies on the order of 100% [15]. The interpretation of $0\nu 2\beta$ experiments relies on reliable calculations of the nuclear matrix elements, with robust uncertainty estimation. While the heavy nuclei system is beyond the capability of the current lattice QCD calculation, computations of the double beta decay for a light nuclei system shall be feasible [16, 17]. The lattice results are required as inputs to determine the relevant low energy constants in the effective field theory [18–21], with which the nuclear matrix elements for heavy nuclei system can be calculated.

Without the signal-to-noise-ratio problem, the decay channels $\pi^-\pi^- \rightarrow ee$ and $\pi^- \rightarrow \pi^+ ee$ serve as an ideal laboratory to perform a lattice QCD study of the $0\nu 2\beta$ decay and to test the prediction from effective field theory. Our exploratory study [2] has demonstrated the possibility of a first-principles calculation of the $\pi^-\pi^- \rightarrow ee$ decay, where we obtained the decay amplitude

$$\frac{\mathcal{A}(\pi\pi \rightarrow ee)}{\mathcal{A}^{LO}} \Big|_{m_\pi=420 \text{ MeV}} = 0.759(6)_{\text{stat}}, \quad \frac{\mathcal{A}(\pi\pi \rightarrow ee)}{\mathcal{A}^{LO}} \Big|_{m_\pi=140 \text{ MeV}} = 0.910(3)_{\text{stat}}, \quad (1)$$

with \mathcal{A}^{LO} the leading-order prediction from chiral perturbation theory (χ PT). By putting the amplitude into the χ PT formula [18]

$$\frac{\mathcal{A}(\pi\pi \rightarrow ee)}{\mathcal{A}^{LO}} = 1 - \frac{m_\pi^2}{(4\pi F_\pi)^2} \left(3 \log \frac{\mu^2}{m_\pi^2} + \frac{7}{2} + \frac{\pi^2}{4} + \frac{5}{6} g_\nu^{\pi\pi}(\mu) \right), \quad (2)$$

we obtain the low energy constant $g_\nu^{\pi\pi}(\mu)$ at $\mu = m_\rho = 775$ MeV

$$g_\nu^{\pi\pi}(m_\rho)\Big|_{m_\pi=420 \text{ MeV}} = -8.50(9)_{\text{stat}}, \quad g_\nu^{\pi\pi}(m_\rho)\Big|_{m_\pi=140 \text{ MeV}} = -11.96(31)_{\text{stat}}, \quad (3)$$

where the uncertainties are statistical only. The two values of $g_\nu^{\pi\pi}$ differ by $\sim 30\%$. This can be accounted by the systematic effects in the lattice calculation such as finite-volume effects and lattice artifacts, as well as higher-order truncation effects from χ PT.

The lattice QCD calculations of $\pi^- \rightarrow \pi^+ ee$ decay have been first carried out by CallLat Collaboration [22] for the short-distance contribution and NPLQCD Collaboration [23] for the long-distance contribution. While the vanishing phase space does not allow the $\pi^- \rightarrow \pi^+ ee$ decay happen in nature (This problem does not exist for the $K^- \rightarrow \pi^+ ee$ decay, which is proposed by Ref. [24]), the hadronic matrix element is well defined within the Standard Model and is equivalent to the one from $\pi^- e^+ \rightarrow \pi^+ e^-$ scattering, where π^\pm and e^\pm carry zero spatial momentum. As the crossed-channel analog to the $\pi^- \pi^- \rightarrow ee$ decay, the process of $\pi^- \rightarrow \pi^+ ee$ can be combined together with $\pi^- \pi^- \rightarrow ee$ and serves as a cross-check for the prediction from χ PT. Since in $\pi^- \rightarrow \pi^+ ee$ decay the initial and final state only involves a single stable hadron, the study of the finite-volume effects is simplified. For example, we can adopt a newly developed technique called infinite-volume reconstruction [1] to determine the decay amplitude, where the finite-volume effects are exponentially suppressed even a massless neutrino propagator is included in the lattice calculation. Using four ensembles with different volumes and lattice spacings, we obtain the decay amplitude as

$$\frac{\mathcal{A}(\pi^- \rightarrow \pi^+ ee)}{\mathcal{A}^{LO}}\Big|_{m_\pi=140 \text{ MeV}} = 1.1045(34)_{\text{stat}}(74)_{\text{sys}}, \quad (4)$$

where the first uncertainty is statistical and the second one is an estimation for both finite-volume effects and lattice artifacts. Using the χ PT formula for $\pi^- \rightarrow \pi^+ ee$ decay [18]

$$\frac{\mathcal{A}(\pi^- \rightarrow \pi^+ ee)}{\mathcal{A}^{LO}} = 1 + \frac{m_\pi^2}{(4\pi F_\pi)^2} \left(3 \log \frac{\mu^2}{m_\pi^2} + 6 + \frac{5}{6} g_\nu^{\pi\pi}(\mu) \right) \quad (5)$$

we obtain the low energy constant

$$g_\nu^{\pi\pi}(m_\rho)\Big|_{m_\pi=140 \text{ MeV}} = -10.89(28)_{\text{stat}}(74)_{\text{sys}}. \quad (6)$$

Although the functional forms of χ PT formulae (2) and (5) are quite different, the results for $g_\nu^{\pi\pi}$ given in (3) and (6) are close to each other, demonstrating the success of χ PT prediction.

II. CALCULATION OF $0\nu 2\beta$ PROCESS: $\pi^- \rightarrow \pi^+ ee$

The decay amplitude of a general $0\nu 2\beta$ process $I(p_I) \rightarrow F(p_F)e(p_1)e(p_2)$ can be written as

$$\mathcal{A} = \langle F, e_1, e_2 | \mathcal{H}_{\text{eff}} | I \rangle. \quad (7)$$

Here we use $e_{1,2}$ to specify the electron state carrying momentum $p_{1,2}$. The second-order weak effective Hamiltonian is defined as

$$\begin{aligned} \mathcal{H}_{\text{eff}} &= \frac{1}{2!} \int d^4x T[\mathcal{L}_{\text{eff}}(x)\mathcal{L}_{\text{eff}}(0)], \\ \mathcal{L}_{\text{eff}} &= 2\sqrt{2}G_F V_{ud}(\bar{u}_L \gamma_\mu d_L)(\bar{e}_L \gamma_\mu \nu_{eL}). \end{aligned} \quad (8)$$

Here G_F is the Fermi constant and V_{ud} is the CKM matrix element. The left-handed fermion fields are defined as $\psi_L = P_L \psi$, $\bar{\psi}_L = \bar{\psi} P_R$ (for $\psi = u, d, e, \nu_e$) with projectors $P_{L,R} = (1 \mp \gamma_5)/2$.

The effective Hamiltonian can be written as a product of hadronic and leptonic factors

$$\mathcal{H}_{\text{eff}} = H_{\mu\nu}(x)L_{\mu\nu}(x), \quad (9)$$

where the hadronic factor $H_{\mu\nu}(x)$ is defined as $H_{\mu\nu}(x) = T[J_{\mu L}(x)J_{\nu L}(0)]$ with $J_{\mu L}(x) = \bar{u}_L \gamma_\mu d_L(x)$. Under the mechanism that $0\nu 2\beta$ decays are mediated by the exchange of light Majorana neutrinos, the leptonic factor $L_{\mu\nu}(x)$ is given by

$$L_{\mu\nu}(x) = -4G_F^2 V_{ud}^2 m_{\beta\beta} S_0(x) \bar{e}_L(x) \gamma_\mu \gamma_\nu e_L^c(0), \quad (10)$$

where $S_0(x) = \int \frac{d^4q}{(2\pi)^4} \frac{e^{iqx}}{q^2}$ denotes a massless scalar propagator and the effective neutrino mass $m_{\beta\beta} = |\sum_i U_{ei}^2 m_i|$ combines the neutrino masses m_i and the elements U_{ei} of the Pontecorvo-Maki-Nakagawa-Sato (PMNS) matrix. The charge conjugate of a fermionic field ψ is given as $\psi^c = C\bar{\psi}^T = \gamma_4 \gamma_2 \bar{\psi}^T$.

A. Decay amplitude of $\pi^- \rightarrow \pi^+ ee$

For specific process $\pi^- \rightarrow \pi^+ ee$, with two electrons carrying vanishing momenta, the decay amplitude in Minkowski space-time becomes

$$\mathcal{A}^M = -2T_{\text{lept}} \int d^4x H^M(x) S_0^M(x) \quad (11)$$

where leptonic part is factorized in $T_{\text{lept}} = 4G_F^2 V_{ud}^2 m_{\beta\beta} \bar{e}_L(p_1) e_L^c(p_2)$. The superscript M denotes the Minkowski space-time. The factor of 2 comes from interchange of electrons. The hadronic function is defined by

$$H^M(x) = \langle \pi^+ | T \{ J_{\mu L}^M(x) J_{\mu L}^M(0) \} | \pi^- \rangle. \quad (12)$$

This calculation is similar to the calculation of QED corrections to self energy using Feynman gauge. We can adopt the infinite-volume reconstruction (IVR) method proposed in Ref. [1] to compute the $\pi^- \rightarrow \pi^+ ee$ transition amplitude.

It should be noted that the hadronic function receives contribution from the vacuum state, which is lighter than the single pion state. In the Euclidean space-time, the hadronic function would grow exponentially as the time separation between the two current operators increases. To reproduce the amplitude in Eq. (11), one needs to treat the vacuum state properly as we will describe later.

In the following sections, we will first introduce our approach to calculate the Euclidean space-time hadronic function $H(x)$ on lattice (For simplicity, we have left out the superscript of E for Euclidean space-time) and connect it with the Minkowski space-time integral, Eq. (11). Then we use two different methods, QED_L and IVR, to calculate the integral in Eq. (11). The results from the two methods are compared and discussed later.

B. Calculation of the hadronic function

In order to calculate the Euclidean space-time hadronic function on lattice, we define the following four point correlation function

$$C(t_f, x, y, t_i) = \langle \phi_{\pi^+}(t_f) J_{\mu L}(x) J_{\mu L}(y) \phi_{\pi^-}^\dagger(t_i) \rangle \quad (13)$$

with wall-source pion interpolating operators $\phi_{\pi^-}^\dagger$ and ϕ_{π^+} . Here the time slices t_i and t_f are chosen as

$$t_i = \min(x_t, y_t) - \Delta T, \quad t_f = \max(x_t, y_t) + \Delta T \quad (14)$$

with sufficiently large ΔT for the ground-state saturation. Since the wall-source operators have a good overlap with the π ground state, we find the ground-state saturation for $\Delta T \gtrsim 1$

Ensemble	m_π [MeV]	$L^3 \times T$	a^{-1} [GeV]	N_{conf}	$m_\pi L$	$\Delta T/a$
24D	142	$24^3 \times 64$	1.015	91	3.3	8
32D	142	$32^3 \times 64$	1.015	56	4.5	8
32D-fine	143	$32^3 \times 64$	1.378	24	3.3	10
48I	139	$48^3 \times 96$	1.73	34	3.9	12

Table I. Ensembles used in this work are generated by the RBC/UKQCD collaborations [25, 26]. We list the pion mass m_π , the space-time volume $L^3 \times T$, the lattice spacing a , the number, N_{conf} , of configurations used, the values of $m_\pi L$ and the time separation, ΔT , used for the π ground-state saturation.

fm at the physical pion mass. For the ensembles used in this work, the values of ΔT are chosen conservatively and listed in Table I.

The Euclidean space-time hadronic function is given by:

$$H(x-y) = V \frac{C(t_f, x, y, t_i)}{C_\pi(t_f, t_i)}, \quad C_\pi(t_f, t_i) = \langle \phi_{\pi^-}(t_f) \phi_{\pi^-}^\dagger(t_i) \rangle \quad (15)$$

where $V = L^3$ is the spatial-volume factor. In $H(x-y)$ the vacuum-intermediate-state contribution from $\langle \pi^+ | J_{\mu L}(x) | 0 \rangle \langle 0 | J_{\mu L}(y) | \pi^- \rangle$ leads to an exponentially growing factor $e^{m_\pi(t_x - t_y)}$ in Euclidean correlator when $t_x - t_y$ increases. Here, we define the subtracted Euclidean space-time hadronic function:

$$H'(x) = H(x) - H_0(x), \quad (16)$$

with $H_0(x)$ defined as

$$H_0(x-y) = V \frac{C_0(t_f, x, y, t_i)}{C_\pi(t_f, t_i)}, \quad (17)$$

$$C_0(t_f, x, y, t_i) = \langle \phi_{\pi^+}(t_f) J_{\mu L}(x) \rangle \langle J_{\mu L}(y) \phi_{\pi^-}^\dagger(t_i) \rangle + \langle \phi_{\pi^+}(t_f) J_{\mu L}(y) \rangle \langle J_{\mu L}(x) \phi_{\pi^-}^\dagger(t_i) \rangle.$$

The contractions of correlation function $C(t_f, x, y, t_i)$ are given by the *type1* and *type2* diagrams in Fig. 1, while the contractions of $C_0(t_f, x, y, t_i)$ are given by the *vacuum* diagram, where the two hadronic parts are only connected through a neutrino propagator. It should be noted that either $x_t < y_t$ or $x_t > y_t$ are possible. After the subtraction, we remove the unphysical, exponentially-growing contributions.

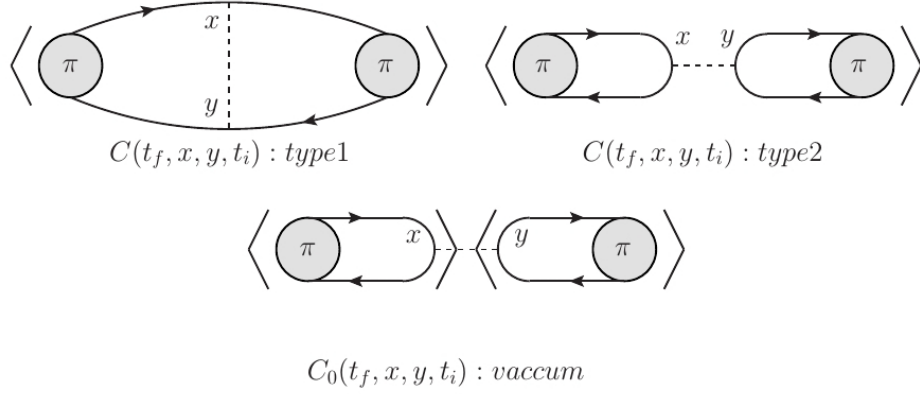


Figure 1. Contractions of correlation function $C(t_f, x, y, t_i)$ and $C_0(t_f, x, y, t_i)$.

In Minkowski space-time, the amplitude contributed by the *vacuum* diagram, \mathcal{A}_0^M , are known analytically and takes the simple form as

$$\mathcal{A}_0^M = -2T_{\text{lept}}F_\pi^2, \quad (18)$$

where the decay constant F_π is defined as

$$\langle 0 | (\bar{u}\gamma_\mu\gamma_5 d)^M | \pi^-(p) \rangle = i\sqrt{2}p_\mu F_\pi. \quad (19)$$

Comparing \mathcal{A}_0^M with the χ PT formula [18]

$$\mathcal{A}_{\chi PT} = 2T_{\text{lept}}F_\pi^2 \left[1 + \frac{m_\pi^2}{(4\pi F_\pi)^2} \left(3 \log \frac{\mu^2}{m_\pi^2} + 6 + \frac{5}{6}g_\nu^{\pi\pi}(\mu) \right) \right] \quad (20)$$

we can find that \mathcal{A}_0^M is just the leading order term in χ PT.

In the Euclidean space-time, although H_0 function cannot reproduce the physical vacuum contribution \mathcal{A}_0^M , by removing it and using the hadronic function $H'(x)$ as inputs, we can obtain the subtracted amplitude, $\mathcal{A}' = \mathcal{A}^M - \mathcal{A}_0^M$, which includes the higher-order χ PT contributions. Through out the paper, we will calculate the dimensionless, normalized amplitude A

$$A = \frac{\mathcal{A}'}{\mathcal{A}_0^M} \equiv -\frac{1}{F_\pi^2} \int d^4x H'(x)S_0(x), \quad (21)$$

which can be used to determine low energy constant $g_\nu^{\pi\pi}$ via

$$A = \frac{m_\pi^2}{(4\pi F_\pi)^2} \left(3 \log \frac{\mu^2}{m_\pi^2} + 6 + \frac{5}{6}g_\nu^{\pi\pi}(\mu) \right) + O\left(\frac{m_\pi^2}{(4\pi F_\pi)^2} \right)^2. \quad (22)$$

C. Lattice setup

We use four ensembles at the physical pion mass generated by the RBC and UKQCD Collaborations [25, 26]. The corresponding parameters are listed in Table I. For the ensembles 24D and 32D, lattice spacings are the same but the lattice volumes are different. It allows us to study the finite-volume effects. The ensemble 48I, 32D-fine and 24D have different lattice spacings but similar volumes. These ensembles provide us the information to examine the lattice artifacts. Note that the 48I uses Iwasaki gauge action in the simulation while the other three ensembles use Iwasaki+DSDR action.

We produce wall-source light-quark propagators on all time slices and make use of the time translation invariance to average the correlator over all T time translations. We have used AMA [27] and low modes deflation with compressed eigen-vectors [28]. These techniques have greatly reduced the computational cost for generating propagators. The correlators for the *type1* and *type2* diagrams in Fig. 1 are given by

$$\begin{aligned} C_{type1}(x-y) &= \text{Tr} [\gamma_5 S(t_f; x) \gamma_{\mu L} S(x; t_i) \gamma_5 S(t_i; y) \gamma_{\mu L} S(y; t_f)] + \{x \leftrightarrow y\} \\ C_{type2}(x-y) &= -\text{Tr} [\gamma_5 S(t_i; x) \gamma_{\mu L} S(x; t_i)] \text{Tr} [\gamma_5 S(t_f; y) \gamma_{\mu L} S(y; t_f)] + \{x \leftrightarrow y\}, \end{aligned} \quad (23)$$

where S the light-quark propagator. We can write the above correlator in a general form of

$$C(x-y) = H_1(x)H_2(y). \quad (24)$$

Such form allows us to obtain a spatial volume average of $C(x)$ by using the double Fourier transformation. We have

$$\begin{aligned} C(x) &= \frac{1}{V} \sum_{\vec{y}} H_1(x+y)H_2(y) \\ &= \frac{1}{V} \sum_{\vec{y}} \left(\frac{1}{V} \sum_{\vec{p}} \tilde{H}_1(t_x, \vec{p}) e^{i\vec{p} \cdot (\vec{x} + \vec{y})} \right) \left(\frac{1}{V} \sum_{\vec{q}} \tilde{H}_2(t_y, \vec{q}) e^{i\vec{q} \cdot \vec{y}} \right) \\ &= \frac{1}{V} \left(\frac{1}{V} \sum_{\vec{p}} \tilde{H}_1(t_x, \vec{p}) \tilde{H}_2(t_y, -\vec{p}) e^{i\vec{p} \cdot \vec{x}} \right) \end{aligned} \quad (25)$$

where $\tilde{H}_i(t, \vec{p})$ ($i = 1, 2$) is a spatial Fourier transformation of $H_i(t, \vec{x})$. Using the spatial volume average, we can obtain a precise lattice data for both connected (*type1*) and disconnected (*type2*) diagrams.

D. The infinite volume reconstruction and QED_L method

As pointed out earlier, the calculation of $\pi^- \rightarrow \pi^+ ee$ transition is similar with the one of QED self energy contributions to $\pi^+ - \pi^0$ mass difference. So we adopt both methods of QED_L and IVR in our analysis, although no QED effects are involved here. Note that a particularity of double beta decay is that the $J_{\mu L}$ interpolating operator involves both vector (V) and axial-vector (A) currents. The VA+AV contributions vanish due to the parity symmetry. After combining the VV and AA contributions, we obtain a large cancellation in $\pi^- \rightarrow \pi^+ ee$ transition amplitude and a significant reduction in its uncertainty. As a result, the finite-volume (FV) effects are enhanced compared to the statistical errors.

1. QED_L

We start the calculation of the normalized amplitude A defined in Eq. (21) using the QED_L method, first introduced in Ref. [29]

$$A = A_{\text{QED}_L} + \delta_{\text{QED}_L}(L) = -\frac{1}{F_\pi^2} \int_{VT} d^4x H_{\text{lat}}(x) S_{\text{lat}}(x) + \delta_{\text{QED}_L}(L), \quad (26)$$

where the integral $\int_{VT} d^4x$ indicates that the integral is performed within a space-time volume $V \times T$. $H_{\text{lat}}(x)$ is a lattice version of $H(x)$ function defined in Eq. (12) and the scalar propagator is given by $S_{\text{lat}}(x) = \frac{1}{VT} \sum_{p_0} \sum_{\vec{p} \neq \vec{0}} \hat{S}_{\text{lat}}(p) e^{ipx}$ with $\hat{S}_{\text{lat}}(p) = \frac{1}{\sum_i \hat{p}_i^2}$ and $\hat{p}_i = 2 \sin(p_i/2)$. Note that the zero mode has been removed from $S_{\text{lat}}(x)$. The corresponding FV effects $\delta_{\text{QED}_L}(L)$ are known to be power-law suppressed. The contribution from H_0 is automatically removed as it is associated with the zero mode of neutrino propagator.

For the VV part of amplitude, $O(1/L)$ and $O(1/L^2)$ corrections in $\delta_{\text{QED}_L}(L)$ come from the π intermediate state. These corrections are universal and known as [30, 31]

$$\delta_{\text{QED}_L}^{VV,LO}(L) = \frac{1}{F_\pi^2} \frac{m_\pi c_1}{4\pi L}, \quad \delta_{\text{QED}_L}^{VV,NLO}(L) = \frac{1}{F_\pi^2} \frac{c_1}{2\pi L^2}, \quad (27)$$

where $c_1 = 2.83729$. For the AA part, the FV corrections arise from the excited states, e.g. $\pi\pi$, and are at the order of $O(1/L^2)$. These contributions are not described by the scalar QED and cannot be simply given by a function of m_π and L . So in our analysis we only consider the $O(1/L)$ or partially $O(1/L^2)$ FV corrections given in Eq. (27).

2. Infinite volume reconstruction

The detailed description of the IVR method have been given in Ref. [1], where the time integral is split into the range of $|t| > t_s$ and $|t| < t_s$

$$\begin{aligned}
A &= A(|t| < t_s) + A(|t| > t_s) \\
&= -\frac{1}{F_\pi^2} \left(\int_{|t| < t_s} d^4x H'(x)S(x) + \int_{|t| > t_s} d^4x H'(x)S(x) \right) \\
&= -\frac{1}{F_\pi^2} \left(\int_{|t| < t_s} d^4x H'(x)S(x) + \int d^3x H'(t_s, \vec{x})L(t_s, \vec{x}) \right) \\
&= -\frac{1}{F_\pi^2} \left(\int_{V, |t| < t_s} d^4x H'_{\text{lat}}(x)S(x) + \int_V d^3x H'_{\text{lat}}(t_s, \vec{x})L(t_s, \vec{x}) \right) + \delta_{\text{IVR}}(L) \\
&\equiv A_{\text{IVR}} + \delta_{\text{IVR}}(L).
\end{aligned} \tag{28}$$

Here a time t_s ($t_s \lesssim L$) is chosen to be sufficiently large for the intermediate π -state saturation. As a result the hadronic function $H'(t, \vec{x})$ at $|t| > t_s$ can be related to $H'(t_s, \vec{x})$ using the ground-state dominance. Therefore the integral of $\int_{|t| > t_s} d^4x H'(x)S(x)$ in the second line of Eq. (28) can be written as $\int d^3x H'(t_s, \vec{x})L(t_s, \vec{x})$ in the third line, with the weighting function $L(t_s, \vec{x})$ given by

$$L(t_s, \vec{x}) = \frac{1}{(2\pi)^2} \int_0^\infty dp \frac{\sin(p|\vec{x}|)}{(E_p + p - m_\pi)|\vec{x}|} e^{-pt_s}. \tag{29}$$

In the fourth line of Eq. (28) the spatial integrals in the infinite volume $\int d^3x$ are replaced by the finite-volume integral $\int_V d^3x$. Besides, the hadronic function $H'(x)$ in the integrand are replaced by the finite-volume lattice data $H'_{\text{lat}}(x)$. According to the above changes, the FV corrections $\delta_{\text{IVR}}(L)$ account for two effects: 1) the difference between $H'_{\text{lat}}(x)$ and $H'(x)$ inside the spacetime box where lattice data are available, 2) the integral outside the spatial volume V , where lattice data are not available. Both effects are exponentially suppressed as demonstrated in Ref. [1]. Thus for sufficiently large volume, we can ignore $\delta_{\text{IVR}}(L)$.

In this calculation, the lattice volumes listed in Table I are relatively small. Besides, FV effects are enhanced due to the cancellation between VV and AA contributions. As a consequence, even exponentially suppressed, the size of $\delta_{\text{IVR}}(L)$ are statistically significant. This can be confirmed by Fig. 2, where we compare the amplitude A_{IVR} for ensembles 24D and 32D. Although VV and AA parts of the amplitudes are nearly consistent for the two ensembles, a significant discrepancy is found after the VV and AA parts are combined together.

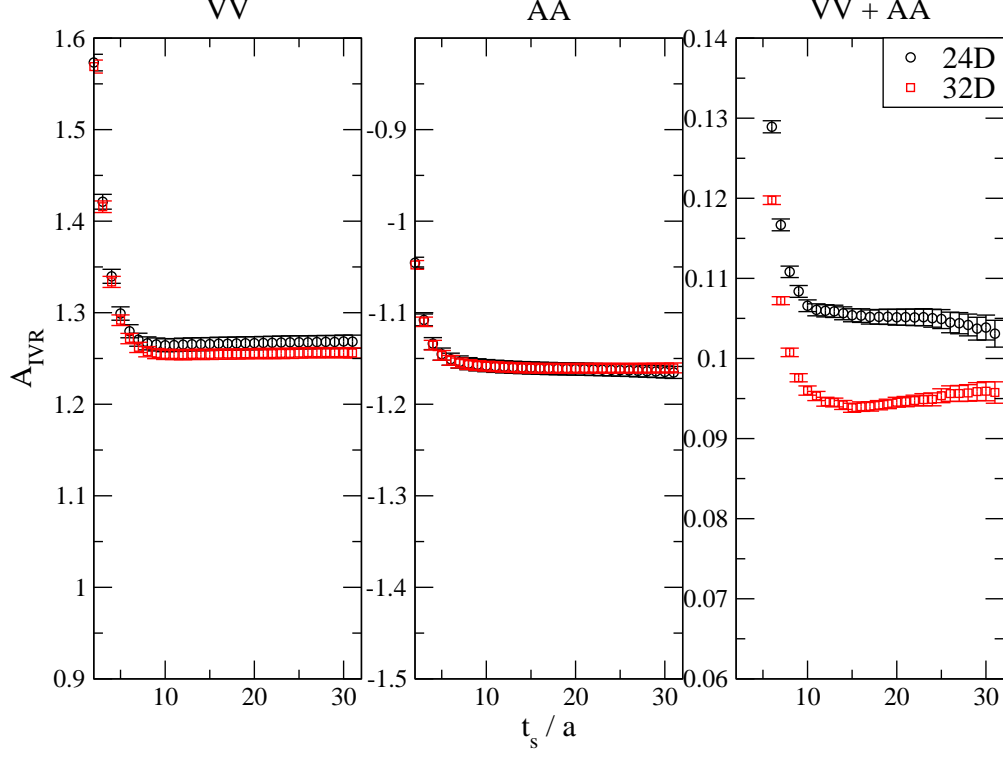


Figure 2. The amplitude A_{IVR} as a function of t_s for ensembles 24D (black circle) and 32D (red cubic). The left, middle and right panels show the results for the VV, AA and VV+AA contributions, respectively. Due to the cancellation between VV and AA contributions, the finite-volume effects in the combined results become significant when compared to the statistical errors.

Due to the enhanced FV effects, it is necessary to estimate the size of $\delta_{\text{IVR}}(L)$ in our calculation. Note that $\delta_{\text{IVR}}(L)$ receives the dominant contributions from pion intermediate states. The relevant hadronic function can be written as

$$\begin{aligned}
 H_\pi(x) &= \int \frac{d^3p}{(2\pi)^3 2E_{\pi,\vec{p}}} \langle \pi^+(0) | J_{\mu L}(0) | \pi^0(p) \rangle \langle \pi^0(p) | J_{\mu L}(0) | \pi^-(0) \rangle e^{i\vec{p}\cdot\vec{x}} e^{-(E_{\pi,\vec{p}} - m_\pi)|t|} \\
 &= - \int \frac{d^3p}{(2\pi)^3 2E_{\pi,\vec{p}}} m_\pi (m_\pi + E_{\pi,\vec{p}}) [F_\pi(q^2)]^2 e^{i\vec{p}\cdot\vec{x}} e^{-(E_{\pi,\vec{p}} - m_\pi)|t|},
 \end{aligned} \tag{30}$$

where $F_\pi(q^2)$ is the pion form factor with $q^2 = 2m_\pi(m_\pi - E_{\pi,\vec{p}})$ and $E_{\pi,\vec{p}} = \sqrt{m_\pi^2 + \vec{p}^2}$. The corresponding hadronic function in the finite volume is then given by

$$H_\pi^{(L)}(x) = - \frac{1}{L^3} \sum_{\vec{p}} \frac{1}{2E_{\pi,\vec{p}}} m_\pi (m_\pi + E_{\pi,\vec{p}}) [F_\pi(q^2)]^2 e^{i\vec{p}\cdot\vec{x}} e^{-(E_{\pi,\vec{p}} - m_\pi)|t|}. \tag{31}$$

Using the pion contribution as input, we can approximate $\delta_{\text{IVR}}(L)$ by

$$\delta_{\text{IVR}}(L) \approx \delta_{\text{IVR}}^\pi(L) = A_{\text{IVR}}^\pi - A_{\text{IVR}}^\pi(L) \tag{32}$$

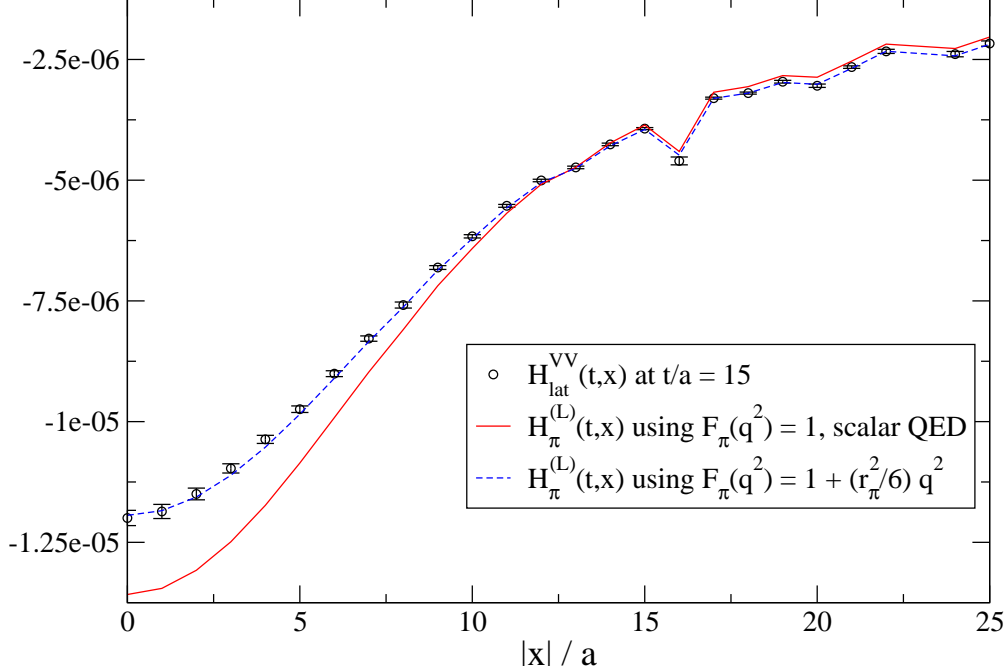


Figure 3. The VV part of the hadronic function $H_{\text{lat}}^{VV}(t, \vec{x})$ at $t/a = 15$ as a function of $|\vec{x}|$. A comparison is made between lattice data of $H_{\text{lat}}^{VV}(t, \vec{x})$ and the pion contribution $H_{\pi}^{(L)}(t, \vec{x})$ by setting $F_{\pi}(q^2) = 1$ and $F_{\pi}(q^2) = 1 + (r_{\pi}^2/6)q^2$.

where A_{IVR}^{π} and $A_{\text{IVR}}^{\pi}(L)$ are determined using the hadronic functions $H_{\pi}(x)$ and $H_{\pi}^{(L)}(x)$, respectively. Depending on the functional forms of $F_{\pi}(q^2)$, we have two estimates for $\delta_{\text{IVR}}^{\pi}$.

- In the framework of scalar QED, we set $F_{\pi}(q^2) = 1$, where the internal electromagnetic structure of pion is neglected. As shown in Fig. 3, at large t and \vec{x} , e.g. $t/a = 15$ and $|\vec{x}|/a > 12$, the lattice results of the VV hadronic function $H_{\text{lat}}^{VV}(x)$ agree relatively well with the $H_{\pi}^{(L)}(x)$ from scalar QED. We denote the $\delta_{\text{IVR}}^{\pi}$ using $F_{\pi}(q^2) = 1$ as $\delta_{\text{IVR}}^{\pi,(1)}$.
- If we adopt the expression of $F_{\pi}(q^2) = 1 + (r_{\pi}^2/6)q^2$ and use the PDG value of the pion charge radius $r_{\pi} = 0.659(4)$ fm as input [32], a better consistency is found between the lattice data of $H_{\text{lat}}^{VV}(x)$ and $H_{\pi}^{(L)}(x)$ at $t/a = 15$. In this case, $\delta_{\text{IVR}}^{\pi}$ is denoted as $\delta_{\text{IVR}}^{\pi,(2)}$.

From Fig. 3 we confirm that the long distance behavior of $H_{\text{lat}}^{VV}(x)$ can be well described by the π intermediate state. Since FV effects mainly come from long distance physics, $\delta_{\text{IVR}}^{\pi}(L)$ can provide a good estimate for $\delta_{\text{IVR}}(L)$. It is worthwhile to point out that both $\delta_{\text{IVR}}(L)$ and $\delta_{\text{IVR}}^{\pi}(L)$ are exponentially suppressed as L increases, thus the residual FV effects in

$\delta_{\text{IVR}}(L) - \delta_{\text{IVR}}^\pi(L)$ are also exponentially suppressed and thus well under control.

III. NUMERICAL RESULTS

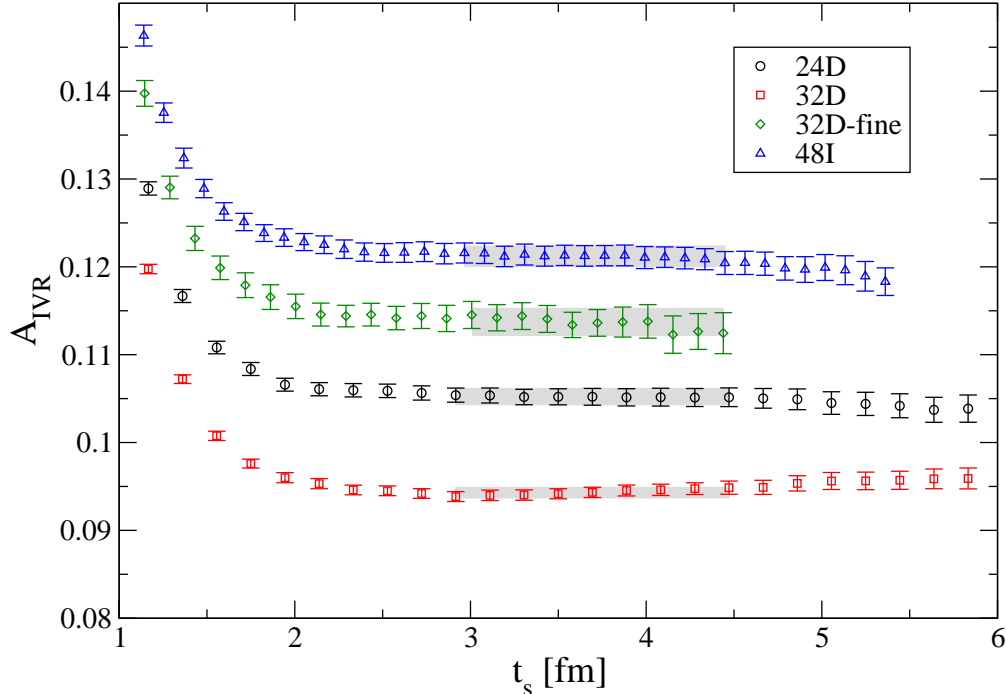


Figure 4. The amplitude A_{IVR} as a function of t_s .

The IVR amplitudes A_{IVR} as a function of t_s are shown in Fig. 4 together with a fit to a constant. All the ensembles shown in Fig. 4 visibly agree with the corresponding fit in the window of $3 \text{ fm} \lesssim t_s \lesssim 4.5 \text{ fm}$ and lead to reasonable values of χ^2 per degree of freedom. The fitting results are shown in Table II.

A. Finite-volume effects

For ensembles 24D ($m_\pi L = 3.3$) and 32D ($m_\pi L = 4.5$), the results A_{IVR} disagree by $\sim 10\%$, which is much larger than their statistical errors. We evaluate the FV corrections $\delta_{\text{IVR}}^{\pi,(1)}$ and $\delta_{\text{IVR}}^{\pi,(2)}$ at $t_s \simeq 3.75 \text{ fm}$ by adopting Eq. (32) and using the input of $F_\pi(q^2) = 1$ and $F_\pi(q^2) = 1 + (r_\pi^2/6)q^2$, respectively. As can be seen in Table II, after adding the corrections, the large discrepancy between 24D and 32D results vanishes. For the ensembles with smallest volume, e.g. 24D and 32D-fine, the results for $A_{\text{IVR}} + \delta_{\text{IVR}}^{\pi,(1)}$ and $A_{\text{IVR}} + \delta_{\text{IVR}}^{\pi,(2)}$ still differ by

Ensemble	A_{IVR}	$A_{\text{IVR}} + \delta_{\text{IVR}}^{\pi,(1)}$	$A_{\text{IVR}} + \delta_{\text{IVR}}^{\pi,(2)}$	$g_{\nu}^{\pi\pi,(0)}$	$g_{\nu}^{\pi\pi,(1)}$	$g_{\nu}^{\pi\pi,(2)}$
24D	0.1052(9)	0.0872(9)	0.0841(10)	-10.63(6)	-12.14(6)	-12.46(7)
32D	0.0943(6)	0.0864(6)	0.0854(6)	-11.53(4)	-12.19(4)	-12.28(5)
32D-fine	0.1137(15)	0.0951(15)	0.0913(14)	-10.04(12)	-11.57(12)	-11.88(12)
48I	0.1212(12)	0.1100(11)	0.1071(12)	-9.27(7)	-10.22(7)	-10.47(8)

Table II. Results of amplitude A_{IVR} and low energy constant $g_{\nu}^{\pi\pi}(\mu)$ at $\mu = m_{\rho}$ for four ensembles. The three columns A_{IVR} , $A_{\text{IVR}} + \delta_{\text{IVR}}^{\pi,(1)}$ and $A_{\text{IVR}} + \delta_{\text{IVR}}^{\pi,(2)}$ correspond to the amplitude without FV correction and the ones with corrections $\delta_{\text{IVR}}^{\pi,(1)}$ and $\delta_{\text{IVR}}^{\pi,(2)}$. The values of $g_{\nu}^{\pi\pi,(0)}$, $g_{\nu}^{\pi\pi,(1)}$ and $g_{\nu}^{\pi\pi,(2)}$ are obtained by putting A_{IVR} , $A_{\text{IVR}} + \delta_{\text{IVR}}^{\pi,(1)}$ and $A_{\text{IVR}} + \delta_{\text{IVR}}^{\pi,(2)}$ into Eq. (22), respectively.

4%, suggesting that the FV effects at the level of $\delta_{\text{IVR}}^{\pi,(2)} - \delta_{\text{IVR}}^{\pi,(1)}$ shall be taken into account in the error budget.

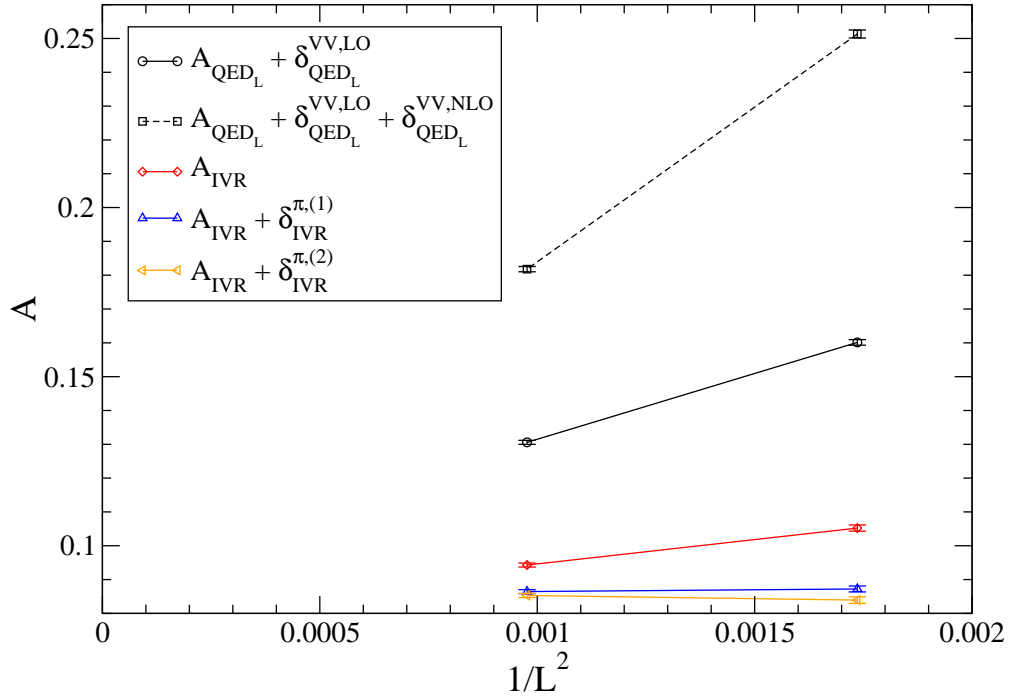


Figure 5. QED_L and IVR results of amplitude A for ensembles 24D and 32D. The black circle and square data are obtained from QED_L method with LO and partially NLO FV corrections given in Eq. (27). The red diamond, blue triangle-up and orange triangle-left data are obtained using IVR method, indicating the amplitude A_{IVR} , $A_{\text{IVR}} + \delta_{\text{IVR}}^{\pi,(1)}$ and $A_{\text{IVR}} + \delta_{\text{IVR}}^{\pi,(2)}$, respectively.

In Fig. 5 we compare the results for ensemble 24D and 32D from QED_L and IVR methods.

With LO and partially NLO FV corrections, the results of $A_{\text{QED}_L} + \delta_{\text{QED}_L}^{VV,LO}$ and $A_{\text{QED}_L} + \delta_{\text{QED}_L}^{VV,LO} + \delta_{\text{QED}_L}^{VV,NLO}$ still have significant dependence on lattice volumes; while for the IVR results, such dependence is very mild. We therefore use the IVR results in the final analysis.

B. Continuum extrapolation

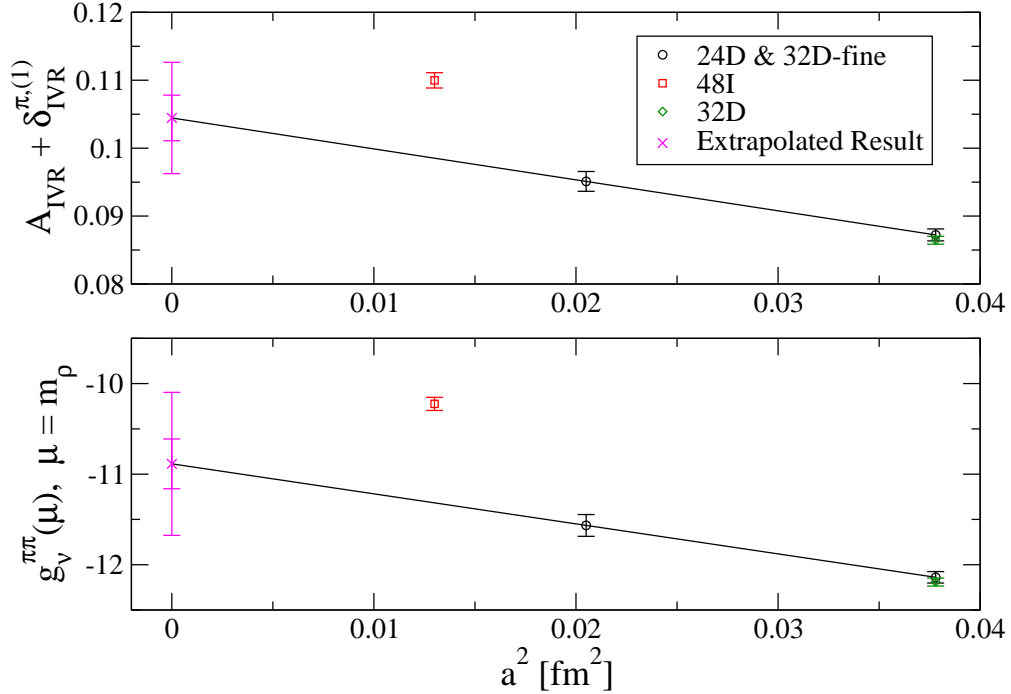


Figure 6. The amplitude $A_{\text{IVR}} + \delta_{\text{IVR}}^{\pi,(1)}$ and the corresponding low energy constant $g_V^{\pi\pi}(\mu)$ at $\mu = m_\rho$ as a function of lattice spacing square.

For all the four ensembles, the amplitude $A_{\text{IVR}} + \delta_{\text{IVR}}^{\pi,(1)}$ as a function of lattice spacing square is shown in Fig. 6. We use the results from 24D ($a^{-1} = 1.015$ GeV) and 32D-fine ($a^{-1} = 1.378$ GeV) ensembles to perform a continuum extrapolation and obtain $A_{\text{IVR}}^{\text{cont}} = 0.1045(34)$ at the continuum limit. We have another ensemble 48I with $a^{-1} = 1.73$ GeV to further examine the lattice artifacts. As the 48I ensemble is simulated with Iwasaki gauge action, it contains the different lattice artifacts compared to the 24D and 32D-fine ensembles, where Iwasaki+DSDR action is used. Although the 48I result cannot be used in the continuum extrapolation directly, it helps us to estimate the size of the lattice artifacts.

C. Results

As we only use two ensembles for continuum extrapolation, the residual lattice artifacts might not be fully controlled by the extrapolation. To be conservative we quote the difference between the extrapolated result $A_{\text{IVR}}^{\text{cont}}$ and the 48I result $A_{\text{IVR}}^{48\text{I}}$ as the size of systematic effects, namely $\delta_a = |A_{\text{IVR}}^{\text{cont}} - A_{\text{IVR}}^{48\text{I}}| = 0.0055$. In Fig. 6 the amplitude at the continuum limit is obtained using $A_{\text{IVR}} + \delta_{\text{IVR}}^{\pi,(1)}$. We also calculate $A_{\text{IVR}} + \delta_{\text{IVR}}^{\pi,(2)}$ using $F_\pi(q^2) = 1 + (r_\pi^2/6)q^2$. The $O(q^2)$ term in $F_\pi(q^2)$ causes a shift $\delta_L = 0.0050$ in the amplitude $A_{\text{IVR}}^{\text{cont}}$. Such effect is included as a systematic uncertainty for the residual FV effects. To sum up, the final result for the amplitude defined in Eq. (21) is given by

$$A = 0.1045(34)(50)_L(55)_a, \quad (33)$$

where the first uncertainty is statistical, the second and third ones are the systematic errors for finite volume and lattice artifacts. Putting the amplitude into Eq. (22), we obtain the results for low energy constant $g_\nu^{\pi\pi}(\mu)$ at $\mu = m_\rho$ with m_ρ the rho meson mass. The values of $g_\nu^{\pi\pi,(0)}$, $g_\nu^{\pi\pi,(1)}$ and $g_\nu^{\pi\pi,(2)}$ are obtained using A_{IVR} , $A_{\text{IVR}} + \delta_{\text{IVR}}^{\pi,(1)}$ and $A_{\text{IVR}} + \delta_{\text{IVR}}^{\pi,(2)}$ as inputs, respectively. These results are put in Table II. Following the similar procedure described above, the final result for $g_\nu^{\pi\pi}$ with both statistical and systematic uncertainties is given by

$$g_\nu^{\pi\pi}(\mu) \Big|_{\mu=m_\rho} = -10.89(28)(33)_L(66)_a. \quad (34)$$

IV. CONCLUSION

We perform a lattice QCD calculation of the amplitude of the neutrinoless double beta decay $\pi^- \rightarrow \pi^+ ee$. The hadronic function $H_0(x)$, which contains the contributions from vacuum state, are subtracted. Such subtraction removes the exponentially growing terms in the Euclidean time integral. The remaining hadronic function $H'(x) = H(x) - H_0(x)$ can be used to determine the normalized amplitude $A = \mathcal{A}^M / \mathcal{A}_0^M - 1$, which can be considered as a fractional deviation between the total decay amplitude \mathcal{A}^M and the leading-order χPT prediction \mathcal{A}_0^M .

In the calculation, we find large FV effects in the decay amplitude. By comparing two approaches, QED_L and IVR, we finally adopt the IVR method in our study, as the associated FV effects are exponentially suppressed and much smaller than that from QED_L. By adding

the FV corrections $\delta_{\text{IVR}}^{\pi,(1)}$ or $\delta_{\text{IVR}}^{\pi,(2)}$ contributed by the pion intermediate state, the 24D and 32D results become consistent. The residual FV effects are estimated by the size of $\delta_{\text{IVR}}^{\pi,(1)} - \delta_{\text{IVR}}^{\pi,(2)}$. After the continuum extrapolation, the final result of A is given in Eq. (33), with a $\sim 3\%$ statistical error. For the systematic effects including both FV effects and lattice artifacts, we estimate them at the level of $\sim 10\%$.

By putting the amplitude A into the χ PT formula, we determine the low energy constant $g_{\nu}^{\pi\pi}$ in Eq. (34). This result is close to the $g_{\nu}^{\pi\pi}$ from $\pi^-\pi^- \rightarrow ee$ decay, which is given in Eq. (3), suggesting that χ PT works well in the pion sector. It has been found in Ref. [20] that a leading-order, short-range contribution needs to be introduced in the $nn \rightarrow ppee$ decay, which breaks down Weinberg's power-counting scheme. Moving the calculation from the pion to the nucleon sector is the next step of our $0\nu 2\beta$ project. It is interesting to examine the impact of this short-range contribution in our future study.

ACKNOWLEDGMENTS

We gratefully acknowledge many helpful discussions with our colleagues from the RBC-UKQCD Collaboration. We warmly thank N. H. Christ, V. Cirigliano, W. Dekens, W. Detmold, E. Mereghetti, D. Murphy, A. Nicholson, U. van Kolck and A. Walker-loud for useful discussion. X.F. and X.-Y.T. were supported in part by NSFC of China under Grant No. 11775002. L.C.J acknowledge support by DOE grant DE-SC0010339. The computation was performed under the ALCC Program of the US DOE on the Blue Gene/Q (BG/Q) Mira computer at the Argonne Leadership Class Facility, a DOE Office of Science Facility supported under Contract DE-AC02-06CH11357. Part of the computation was carried out on facilities of the USQCD Collaboration, which are funded by the Office of Science of the U.S. Department of Energy. The calculation was also carried out on TianHe-1 (A) at Chinese National Supercomputer Center in Tianjin.

[1] X. Feng and L. Jin, (2018), arXiv:1812.09817 [hep-lat].

[2] X. Feng, L.-C. Jin, X.-Y. Tuo, and S.-C. Xia, Phys. Rev. Lett. **122**, 022001 (2019), arXiv:1809.10511 [hep-lat].

- [3] A. Gando *et al.* (KamLAND-Zen), Phys. Rev. Lett. **110**, 062502 (2013), arXiv:1211.3863 [hep-ex].
- [4] M. Agostini *et al.* (GERDA), Phys. Rev. Lett. **111**, 122503 (2013), arXiv:1307.4720 [nucl-ex].
- [5] J. B. Albert *et al.* (EXO-200), Nature **510**, 229 (2014), arXiv:1402.6956 [nucl-ex].
- [6] S. Andringa *et al.* (SNO+), Adv. High Energy Phys. **2016**, 6194250 (2016), arXiv:1508.05759 [physics.ins-det].
- [7] A. Gando *et al.* (KamLAND-Zen), Phys. Rev. Lett. **117**, 082503 (2016), [Addendum: Phys. Rev. Lett.117,no.10,109903(2016)], arXiv:1605.02889 [hep-ex].
- [8] S. R. Elliott *et al.*, *Proceedings, 27th International Conference on Neutrino Physics and Astrophysics (Neutrino 2016): London, United Kingdom, July 4-9, 2016*, J. Phys. Conf. Ser. **888**, 012035 (2017), arXiv:1610.01210 [nucl-ex].
- [9] M. Agostini *et al.*, (2017), 10.1038/nature21717, [Nature544,47(2017)], arXiv:1703.00570 [nucl-ex].
- [10] O. Azzolini *et al.* (CUPID-0), Phys. Rev. Lett. **120**, 232502 (2018), arXiv:1802.07791 [nucl-ex].
- [11] C. E. Aalseth *et al.* (Majorana), Phys. Rev. Lett. **120**, 132502 (2018), arXiv:1710.11608 [nucl-ex].
- [12] J. B. Albert *et al.* (EXO), Phys. Rev. Lett. **120**, 072701 (2018), arXiv:1707.08707 [hep-ex].
- [13] C. Alduino *et al.* (CUORE), Phys. Rev. Lett. **120**, 132501 (2018), arXiv:1710.07988 [nucl-ex].
- [14] M. Agostini *et al.* (GERDA), Phys. Rev. Lett. **120**, 132503 (2018), arXiv:1803.11100 [nucl-ex].
- [15] J. Engel and J. Menéndez, Rept. Prog. Phys. **80**, 046301 (2017), arXiv:1610.06548 [nucl-th].
- [16] P. E. Shanahan, B. C. Tiburzi, M. L. Wagman, F. Winter, E. Chang, Z. Davoudi, W. Detmold, K. Orginos, and M. J. Savage, Phys. Rev. Lett. **119**, 062003 (2017), arXiv:1701.03456 [hep-lat].
- [17] B. C. Tiburzi, M. L. Wagman, F. Winter, E. Chang, Z. Davoudi, W. Detmold, K. Orginos, M. J. Savage, and P. E. Shanahan, Phys. Rev. **D96**, 054505 (2017), arXiv:1702.02929 [hep-lat].
- [18] V. Cirigliano, W. Dekens, E. Mereghetti, and A. Walker-Loud, Phys. Rev. **C97**, 065501 (2018), [Erratum: Phys. Rev.C100,no.1,019903(2019)], arXiv:1710.01729 [hep-ph].
- [19] V. Cirigliano, W. Dekens, J. de Vries, M. L. Graesser, and E. Mereghetti, (2018), arXiv:1806.02780 [hep-ph].
- [20] V. Cirigliano, W. Dekens, J. De Vries, M. L. Graesser, E. Mereghetti, S. Pastore, and U. Van Kolck, Phys. Rev. Lett. **120**, 202001 (2018), arXiv:1802.10097 [hep-ph].

- [21] V. Cirigliano, W. Dekens, J. de Vries, M. L. Graesser, E. Mereghetti, S. Pastore, M. Piarulli, U. van Kolck, and R. B. Wiringa, (2019), arXiv:1907.11254 [nucl-th].
- [22] A. Nicholson *et al.*, (2018), arXiv:1805.02634 [nucl-th].
- [23] W. Detmold and D. J. Murphy, in *36th International Symposium on Lattice Field Theory (Lattice 2018) East Lansing, MI, United States, July 22-28, 2018* (2018) arXiv:1811.05554 [hep-lat].
- [24] Y. Liao and X.-D. Ma, JHEP **03**, 179 (2019), arXiv:1901.10302 [hep-ph].
- [25] T. Blum *et al.* (RBC, UKQCD), Phys. Rev. **D93**, 074505 (2016), arXiv:1411.7017 [hep-lat].
- [26] R. Mawhinney, in *Proceedings, The 36th Annual International Symposium on Lattice Field Theory (LATTICE2018)* (2018).
- [27] E. Shintani, R. Arthur, T. Blum, T. Izubuchi, C. Jung, and C. Lehner, Phys. Rev. **D91**, 114511 (2015), arXiv:1402.0244 [hep-lat].
- [28] M. A. Clark, C. Jung, and C. Lehner, *Proceedings, 35th International Symposium on Lattice Field Theory (Lattice 2017): Granada, Spain, June 18-24, 2017*, EPJ Web Conf. **175**, 14023 (2018), arXiv:1710.06884 [hep-lat].
- [29] M. Hayakawa and S. Uno, Prog. Theor. Phys. **120**, 413 (2008), arXiv:0804.2044 [hep-ph].
- [30] Z. Davoudi and M. J. Savage, Phys. Rev. **D90**, 054503 (2014), arXiv:1402.6741 [hep-lat].
- [31] S. Borsanyi *et al.*, Science **347**, 1452 (2015), arXiv:1406.4088 [hep-lat].
- [32] M. Tanabashi *et al.* (Particle Data Group), Phys. Rev. **D98**, 030001 (2018).